Adsorption Structures of Water in NaX Studied by DRIFT Spectroscopy and Neutron Powder Diffraction

Jens Hunger,*,† Ilir A. Beta,‡ Heinz Böhlig,§ Chris Ling,|| Herve Jobic,⊥ and Bernd Hunger§

Institut für Anorganische Chemie, Universität Leipzig, Johannisallee 29, D-04103 Leipzig, Germany, Department of Physics, Kansas State University, Manhattan, Kansas 66506, Wilhelm-Ostwald-Institut für Physikalische und Theoretische Chemie, Universität Leipzig, D-04103 Leipzig, Germany, School of Chemistry, University of Sydney, NSW 2006, Australia, and Institut de Recherches sur la Catalyse, CNRS, F-69626 Villeurbanne, France

Received: August 17, 2005; In Final Form: August 26, 2005

Diffuse reflectance infrared Fourier transform spectroscopic (DRIFTS) measurements (4000−1500 cm^{-1}) and the results of neutron powder diffraction have been combined to study the structure of adsorption complexes of water in a NaX zeolite at different water loadings (25, 48, 72, and 120 water molecules per unit cell, respectively). Sharp bands corresponding to non-hydrogen-bonded OH groups of water molecules and broad associate bands due to hydrogen-bonded molecules are observed in the DRIFT spectra. We observe a remarkable downshift of the high-frequency associate band in a narrow temperature interval when the water amount decreases from 120 to 72 molecules per unit cell, which could signify some kind of "phase transition" for the water inside the zeolite cavities. Neutron powder diffraction results show that water molecules are predominantly localized in or near the 12-ring windows. Water molecules with hydrogen-bonded and non-hydrogen-bonded OH groups were found, in agreement with the observation of sharp and broad bands in the DRIFT spectra. We find strong evidence for the formation of cyclic hexamers of water molecules localized in the 12-ring windows, which are further stabilized by hydrogen bonds to framework oxygen atoms.

Introduction

The adsorption of water on microporous zeolites is a subject of great scientific and technological interest due to the broad spectrum of zeolite applications as catalysts, adsorbents for separation processes, and ion exchange (e.g., refs 1−5). The influence of zeolite type, aluminum content, exchanged cations, and postsynthesis modifications on the adsorption behavior or pore filling of the zeolites with respect to water have been the scope of numerous experimental studies using different techniques (see, e.g., refs 6−19). In dehydrated zeolites, the extraframework cations that compensate the negative charge of AlO_4^- tetrahedra are localized in certain energetically favorable positions in the framework cavities.[20] However, by using X-ray diffraction techniques, migration of cations between different positions upon adsorption of water has been observed (see, e.g., refs 21−23). Furthermore, more recent studies have shown that adsorption of small amounts of water in zeolites has a significant influence on the adsorption properties of the zeolites with regard to other guest molecules (see, e.g., refs 24−29). Recent theoretical studies have contributed significantly to understanding the adsorption of water in zeolites of different types (see, e.g., refs 30−35). In most cases, the goal of theoretical investigations was to provide insight into the arrangement of water molecules inside the zeolite cavities and their interaction with neighboring water molecules and the zeolite framework. The influence of hydrogen bond formation upon the adsorption behavior of water has also been investigated by theoretical methods.[33]

Temperature-programmed desorption (TPD) experiments for water in faujasites exchanged with alkali-metal cations show stepwise desorption of water as the temperature is increased. At higher temperatures, the shape of the desorption profiles is characteristic for different exchanged cations.[18] Diffuse reflectance infrared Fourier transform spectroscopic (DRIFTS) studies and inelastic neutron scattering (INS) measurements of water in cation-exchanged faujasites hint to the existence of different structures of adsorption complexes depending on the water loading.[36,37] Kirschhock et al. used powder X-ray diffraction for localization of adsorbed water molecules in faujasites at low loadings.[38] Their results show that water molecules sit between two cations and that the structure of adsorption complexes depends on the type of exchanged cation or the presence of more than one type of exchanged cation. However, to our best knowledge, besides X-ray diffraction studies on fully hydrated faujasites (see, e.g., refs 39, 40), no credible results are reported so far in the literature about the arrangement of water molecules and cations at different water loadings in faujasite type zeolites. In this context, vibrational spectroscopic studies can yield significant information because the frequencies and intensities of bands are extremely sensitive to changes in bond geometry and strength that result from adsorption of molecules in zeolite cavities. Electrostatic interactions between cations and guest molecules as well as formation of multiple guest molecule−framework oxygen or guest molecule−guest molecule hydrogen bonds cause significant frequency shifts and changes in band intensity and bandwidth in the vibrational spectra. Knowledge

* Corresponding author. E-mail: che97kdg@studserv.uni-leipzig.de. Telephone: +49 341 9736164. Fax: +49 341 9736249.
† Institut für Anorganische Chemie, Universität Leipzig.
‡ Department of Physics, Kansas State University.
§ Wilhelm-Ostwald-Institut für Physikalische und Theoretische Chemie, Universität Leipzig.
|| School of Chemistry, University of Sydney.
⊥ Institut de Recherches sur la Catalyse.

10.1021/jp054636u CCC: $33.50
Published on Web 12/10/2005

about the localization of water molecules and cations in the zeolite cavities would greatly facilitate the band assignment and the interpretation of IR spectra.

In this contribution, we have used neutron powder diffraction measurements and DRIFT spectroscopy to study the arrangement of water and sodium ions in a NaX zeolite at different water content. We intend to use the results of these "microscopic" techniques for the interpretation at the molecular level of our results for water in NaX obtained with other "macroscopic" methods such as adsorption measurements and already published temperature-programmed desorption (TPD) studies.[17,18]

Experimental Section

Zeolite. The sodium ion-exchanged X-type zeolite with a chemical composition of $Na_{88.1}[Al_{88.1}Si_{103.9}O_{384}]$ and an average crystallite size of 1 μm was commercial product supplied by Chemie AG Bitterfeld/Wolfen (Germany). Nitrogen adsorption measurements at 77 K result in a micropore volume of 0.294 $\pm$ 0.005 $cm^3\ g^{-1}$ (*t*-plot analysis). For TPD and DRIFTS studies, the powder was pressed and granulated to a grain size of 0.2−0.4 mm.

Adsorption Measurements. The adsorption isotherm of water vapor at 298 K was determined gravimetrically on a McBain balance fitted to a high-vacuum system. Under vacuum, 100 mg of the hydrated zeolite powder were activated at 673 K for 20 h. Blank runs were employed to allow for buoyancy effects.

Temperature-Programmed Desorption (TPD). The TPD experiments were carried out in a flow apparatus with helium as the carrier gas (50 $cm^3\ min^{-1}$). For evolved gas detection, both a thermal conductivity detector (TCD) and a quadrupole mass spectrometer (Leybold, Transpector CIS system) with a capillary-coupling system were used. The samples were equilibrated with water vapor over a saturated $Ca(NO_3)_2$ solution in a desiccator. For each experiment, 20 mg of the hydrated zeolite were used in a mixture with 1 g of quartz of the same grain size (0.2−0.4 mm). At first, the samples were flushed with helium at room temperature for 1 h, and then they were heated at 10 K min^{-1} in helium up to 700 K. The desorbed amounts of water were determined by calibration of the TCD signal and the intensity of the 18 amu response.

DRIFT Spectroscopic Studies. The DRIFT spectroscopic experiments were carried out with a System 2000R spectrometer (Perkin-Elmer) by using a Praying Mantis diffuse reflection attachment equipped with a stainless steel reaction chamber (Harrick), which allows temperature-programmed investigations between room temperature and 723 K in a carrier gas flow (helium, 50 $cm^3\ min^{-1}$). The zeolites were equilibrated with water vapor over a saturated $Ca(NO_3)_2$ solution in a desiccator. For each experiment, about 50 mg of the water-loaded zeolite (granulated, 0.2−0.4 mm) were used. At first, the samples were flushed with helium at room temperature for 1 h, and then the linear temperature program (5 K min^{-1}) was started. The spectra were continuously recorded at a resolution of 4 cm^{-1}, with 32 scans being averaged. KBr was used as a standard (background). The spectra were recorded every 10 K; this means that a full measurement consists of a set of 30−40 spectra depending on the investigated zeolite. To test the reproducibility, 2−3 independent measurements were performed on the same zeolite sample. In all cases, they resulted in identical spectra regarding frequencies and intensities. Because the pretreatment of the zeolite samples (1 h flushing with helium, 50 $cm^3\ min^{-1}$ at room temperature) was the same as was used in the previous TPD study,[17,18] the area under the spectra at room temperature has been used for calibration of the adsorbed water amount.

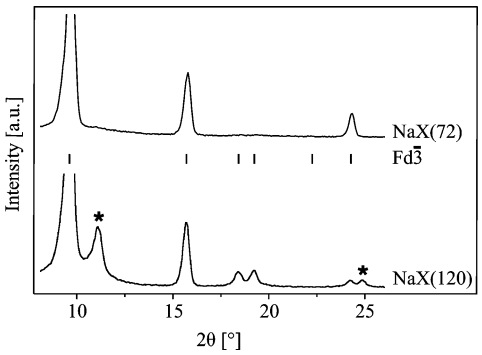

Figure 1. Comparison of the powder diffractograms of samples NaX(72) and NaX(120), showing the problem of indexing NaX(120) in space group $Fd\bar{3}$. Reflections in the powder pattern of NaX(120) that are not consistent with spacegroup $Fd\bar{3}$ are marked with an asterisk.

Neutron Powder Diffraction. *Sample Preparation.* About 5.5 g of the hydrated NaX were activated in glass ampules at 673 K under vacuum. After cooling to room temperature, samples were loaded with predetermined amounts of D_2O. To guarantee a uniform distribution of water molecules inside the zeolite cavities, samples were allowed to equilibrate for 4 h at 373 K. The following samples were studied: NaX(0), NaX(25), NaX(48), NaX(72), and NaX(120), where the specifications in the brackets denote the number of D_2O molecules per unit cell (u.c.). The samples were transferred into airtight cylindrical vanadium cans (15 mm in diameter and 60 mm in height) in a glovebox under helium atmosphere. The cans were sealed with an indium seal.

Data Collection and Structure Refinement. Neutron powder diffraction patterns of the samples were recorded at 5 K on the D2B diffractometer ($\lambda = 2.4$ Å) at the Institute Max von Laue−Paul Langevin (Grenoble, France). The diffraction patterns were analyzed by the Rietveld refinement method[41] by using the GSAS software package.[42] The space group used for samples NaX(0), NaX(25), NaX(48), and NaX(72) was $Fd\bar{3}$ because there was no indication in the powder pattern of a lower symmetry that may have been induced by the adsorption of the water molecules. In the case of the NaX(120) sample, the diffraction pattern cannot be indexed in the space group $Fd\bar{3}$, which indicates the formation of at least one new phase (see Figure 1). Therefore, the powder pattern of this sample was not further analyzed. Because of the highest water content in spacegroup $Fd\bar{3}$, which implies the best chances to find the D_2O molecules in the difference Fourier maps, the structure of NaX(72) was refined at first (see Figure 2). For each sample foremost, the profile parameters, background parameters, zero correction, and lattice constant were refined. After an initial refinement of the framework atoms in NaX(72) with the parameters of the bare zeolite NaX(0) as starting values, the sodium ions and water molecules were located by using difference Fourier maps. The water molecules were refined as rigid bodies with an O−D distance of 0.96 Å and an D−O−D angle of 104°, corresponding to an earlier publication about neutron diffraction on D_2O in BaX.[15] Later, the refined D_2O oxygen positions from NaX(72) were used as starting positions for the refinements of the structures with lower D_2O loadings. In these, after refinement of the framework and occupancies of the Na^+ and D_2O positions as well as Na^+ coordinates, the D_2O rigid bodies were successively allowed to move. This leads to reorientation and repositioning of the D_2O molecules. Any trials to refine the complete structures without rigid body constraints

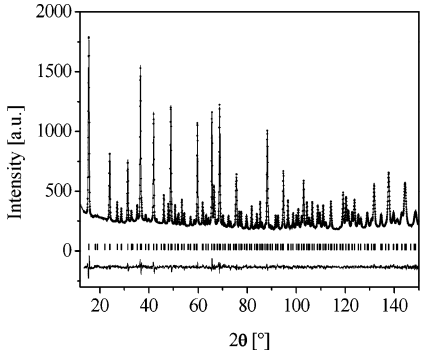

Figure 2. Rietveld plot for the refinement of NaX(72). Upper part: (●), experimental data; (—), calculated profile. Lower part: difference between experimental and calculated profiles.

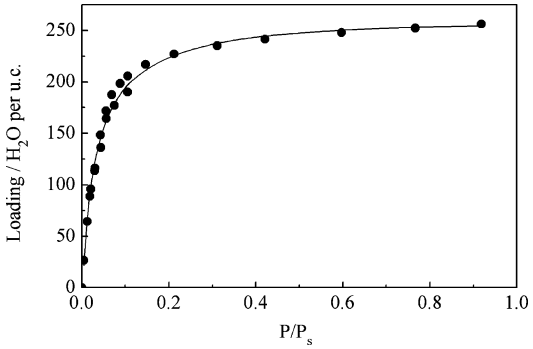

Figure 3. Adsorption isotherm of water on NaX at 298 K: (●), experimental; (—), calculated according eq 1.

lead to divergence because of strong correlations between several parameters and the small data parameter ratio. Structure solution with FOX,[43] whereby framework atoms and cation positions held fixed and cation occupancies and complete water molecules (rigid body coordinates and occupancies) were varied, leads after refinement with GSAS to the same structures. For all samples the low-angle (111) peak was excluded from the refinement because of its significant asymmetric broadening that could not be properly treated by the used software. The experimental conditions and some details of the refinements are specified in Table 1.

Results and Discussion

Adsorption Measurement and Temperature-Programmed Desorption (TPD). The adsorption isotherm of water in NaX at 298 K is shown in Figure 3. The shape of the isotherm that is typical for the adsorption of water in hydrophilic microporous materials corresponds to the Type I of IUPAC classification.[44] At a relative equilibrium pressure of $P/P_s = 0.92$, the adsorbed amount of water is 256 molecules per unit cell (or 32 molecules per supercage). By using the density of liquid water at 298 K, we calculated a total volume of adsorbed water of 0.344 ± 0.005 $cm^3\ g^{-1}$. This calculated volume agrees very well with the theoretical total pore volume of Dubinin et al.[45] (volume of supercages + volume of sodalite cages = 0.349 $cm^3\ g^{-1}$). It can therefore be concluded that, at 298 K and $P/P_s = 0.92$, the pores of NaX zeolite are fully filled with water. The commonly used method of nitrogen adsorption at 77 K yields a pore volume of 0.294 ± 0.005 $cm^3\ g^{-1}$, which is virtually identical to the theoretical volume of supercages of 0.295 $cm^3\ g^{-1}$.[45] This result is indicative of the fact that nitrogen molecules with an apparent kinetic diameter of 0.364 nm cannot enter the sodalite cages because the 6-oxygen-atom ring windows are only 0.26−0.28-nm wide.[1]

Of the total of 256 water molecules adsorbed in NaX at a relative pressure $P/P_s = 0.92$, 71 molecules desorb isothermally during flushing with helium (50 $cm^3\ min^{-1}$) at 298 K for 1 h. The remaining 186 water molecules give rise to the noniso-

TABLE 1: Diffractogram Information[a]

	NaX(0)	NaX(25)	NaX(48)	NaX(72)
	Composition			
water molecules per unit cell	0	18.2(6)	42.8(10)	65.6(13)
	Data Collection			
diffractometer	D2B	D2B	D2B	D2B
temperature [K]	5	5	5	5
wavelength [Å]	2.4	2.4	2.4	2.4
range [deg into Θ]	0−151	0−151	0−151	0−151
stepsize [deg into Θ]	0.05	0.05	0.05	0.05
	Rietveld Refinement			
space group	$Fd\bar{3}$	$Fd\bar{3}$	$Fd\bar{3}$	$Fd\bar{3}$
lattice parameter [Å]	25.09153(18)	25.10741(16)	25.10442(13)	25.05049(15)
profile *R*-factor (R_p)	0.0306	0.0273	0.0239	0.0225
weighted profile *R*-factor (R_{wp})	0.0399	0.0355	0.0312	0.0293
structure *R*-factor (R_F)	0.0233	0.0193	0.0163	0.0194
expected *R*-factor (R_{exp})	0.0211	0.0199	0.0211	0.0201
χ^2	3.636	3.273	2.264	2.215
zero correction [deg]	0.0782(6)	0.0721(5)	0.0733(5)	0.0703(6)
scale factor	2635(7)	2914(6)	2159(5)	2132(6)
number of reflections	410	410	410	404
profile function	pseudo-Voigt			
asymmetry correction	7.89(9)	7.77(7)	7.67(7)	7.38(10)
U	83.9(24)	155(3)	141(2)	85.9(17)
V	−174(3)	−175(3)	−157(2)	−150(3)
W	166.3(15)	158.4(12)	152.3(12)	158.0(15)
background function	20 coefficient shifted Chebychev			

[a] Rietveld refinement was used to minimize $\sum w_i(I_{o,i} - I_{c,i})^2$ where $I_{o,i}$ and $I_{c,i}$ are the observed and calculated powder diffraction intensities for the *i*th point, respectively. Weights, w_i, are $1/I_{o,i}$. Weighted and unweighted profile *R*-factors are defined as $R_{wp} = \{[\sum w_i(I_{o,i} - I_{c,i})^2]/[\sum w_i(I_{o,i})^2]\}^{1/2}$ and $R_p = \sum|I_{o,i} - I_{c,i}|/\sum I_{o,i}$. The structure R_F factor is defined as $R_F = \sum(F_o - F_c)^2]/[\sum(F_o)^2]$. The expected *R*-factor (the statistically best possible value for R_{wp}) is defined as $R_{exp} = [(N - P)/(\sum w_i I_{o,i}^2)]^{1/2}$, where *N* is the number of observed powder diffraction data points and *P* is the number of refined parameters. χ^2 was calculated from $(R_{wp}/R_{exp})^2$.

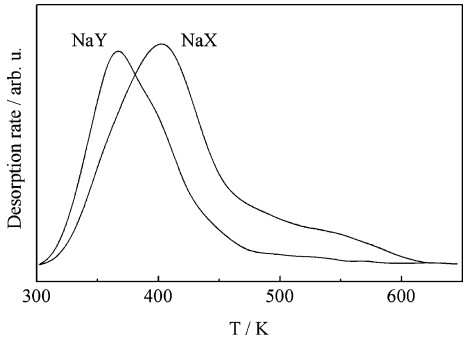

Figure 4. Desorption profiles of water on NaX and NaY (10 K min^{-1}).

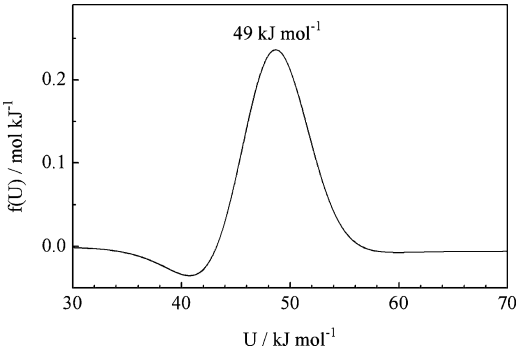

Figure 5. Adsorption energy distribution function of water on the NaX zeolite.

thermal desorption curve (10 K min^{-1}) shown in Figure 4.[17,18] Reversibility of the processes can be assumed because several desorption experiments carried out on one probe showed identical desorption profiles. The desorption curve exhibits a discerned maximum at about 400 K, with a shoulder in the low-temperature part around 370 K. The high-temperature part of the desorption curve has a very characteristic structure with two small but distinguishable peaks at about 490 and 550 K, respectively. The overall structure of the desorption curve of water in NaX indicates a clear dependence of the binding energy on the water loading, i.e., at lower loadings, the binding energy is higher and vice-versa. Such a behavior is caused, in addition to the heterogeneity of the adsorption centers, by changes in the strength of water−sodium cations, water−framework oxygen, and water−water interaction as the loading changes. Decrease of aluminum content, which implies the presence of a smaller number of charge compensating sodium ions (Y-type zeolite), leads to significant changes in the nonisothermal desorption course (see Figure 4). The most obvious change is that, instead of the shoulder at about 370 K for NaX, a clear maximum appears in the case of NaY zeolite at the same position. The shift of the main maximum to lower temperatures indicates a weaker binding of water at high loadings in NaY as compared to NaX zeolite, which is arguably due to the weaker interaction of water molecules with the zeolite framework because of the decrease of the basicity of framework oxygen with decreasing aluminum content.[46] In other words, the hydrophilic properties of the NaY zeolite are less pronounced compared to those of NaX. By visual inspection of Figure 4, it is clearly visible that the amount of water that desorbs at higher temperatures is significantly less in the case of NaY. This could be explained with the smaller number of cations present in NaY given the fact that the course of nonisothermal desorption at higher temperatures is mostly determined by the type and number of exchanged cations.[18]

The heterogeneous structure of zeolites is also responsible for the failure of the simple isotherm fits to describe the adsorption isotherm of water. If a continuous distribution $f(U)$ of adsorption sites with respect to the adsorption energy U is accepted as a quantitative characteristics of an adsorbent's heterogeneity, then the overall coverage $\theta(P,T)$ is expressed by the integral equation:[47,48]

$$\theta(P,T) = \int_{U_{\min}}^{U_{\max}} \theta_{\mathrm{loc}}(P,T,U)\, f(U)\, \mathrm{d}U \qquad (1)$$

where $\theta_{\mathrm{loc}}(P,T,U)$ is the energy-dependent local adsorption isotherm, and $U_{\min}$ and $U_{\max}$ are the limits of the range of adsorption energy. All methods proposed to calculate the adsorption energy distribution from gas adsorption data by means of eq 1 require an assumption of the local isotherm. Without additional information about the system, the model for local adsorption should be as simple as possible. Here, the Langmuir model was applied. The preexponential factor of the Langmuir constant $K_L^o(T)$ is expressed in terms of the partition function for an isolated molecule in the gas and surface phases. As approximation for $K_L^o(T)$, a proposal from literature was used.[49,50] The adsorption energy distribution function $f(U)$ was determined from the experimental adsorption isotherm $\theta(P,T)$ by means of the program INTEG, which involves a regularization method for solving the integral eq 1.[51] The calculations were carried out without any assumptions or constraints on the resulting distribution functions. Thus, negative parts in the distributions are possible. They do not have any special physical meaning, but show the degree of adequacy between the adsorption model used and the experimental data. Therefore, the negative parts in the calculated distribution will not be a matter of interpretation.

The distribution function of the adsorption energies for water in NaX is shown in Figure 5. The width of about 15 kJ mol^{-1} of the unimodal distribution function with its maxium at 49 kJ mol^{-1} is indicative of the energetic heterogeneity of the interaction of water with the zeolite. Adsorption energy values of the lower-energy part of the distribution function are close to the enthalpy of vaporization of water ($\Delta H = 44.0$ kJ mol^{-1} at 298 K),[52] which explains why a significant portion of adsorbed water desorbs isothermally when flushing with helium at 298 K. The higher-energy part of the distribution function exhibits no other structure apart from the discerned maximum at about 49 kJ mol^{-1}, which clearly contradicts the shape of the TPD profile. One should consider, however, that the higher-energy part of the desorption energy distribution function corresponds to the low loading region in which caused by the very low equilibrium pressures adsorption measurements are difficult and prone to significant experimental error. This difficulty is easily overcome in TPD experiments, which yield reliable information mostly in the low loading region.

The observed desorption profiles $r_d(T)$ were analyzed by considering a first-order desorption process with a distribution function $f(E)$ of the effective desorption energy E:[17,18,51,53]

$$r_d(T) = -\frac{\mathrm{d}\theta}{\mathrm{d}t}(T) = A\int_{E_{\min}}^{E_{\max}} \theta_{\mathrm{loc}}(E,T)\exp\left(-\frac{E}{RT}\right) f(E)\, \mathrm{d}E \qquad (2)$$

Here, θ is the overall coverage or loading, and A is an effective preexponential factor. θ_{loc} is the coverage of adsorption sites with desorption energy E, and $E_{\min}$ and $E_{\max}$ are the limits of the desorption energy range. The energy distribution function $f(E)$ was also determined from the experimental desorption curves $r_d(T)$ by means of the program INTEG for solving the integral eq 2.[51,53]

The calculated distribution function of the effective desorption energy for water in NaX is shown in Figure 6. Desorption energy

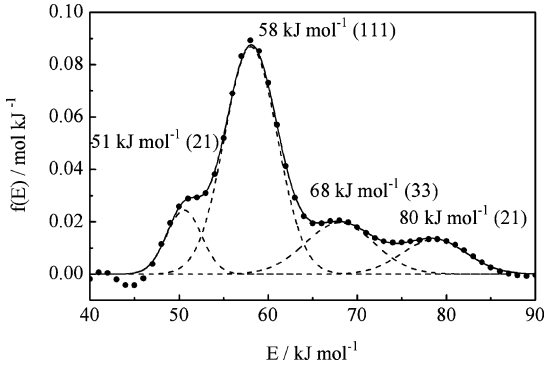

Figure 6. Desorption energy distribution function of water on the NaX zeolite: (●), calculated according eq 2; (—), fitted distribution by four Gaussian peaks; (- - -), single Gaussian peaks (number in brackets denotes the number of water molecules per unit cell).

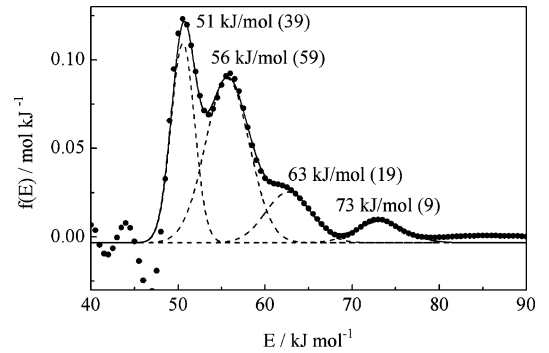

Figure 7. Desorption energy distribution function of water on the NaY zeolite: (●), calculated according eq 2; (—), fitted distribution by four Gaussian peaks; (- - -), single Gaussian peaks (number in brackets denotes the number of water molecules per unit cell).

values for several different loadings are in good agreement with literature data for the adsorption heats of water in NaX determined by microcalorimetric techniques.[19] The distribution function was fitted with 4 Gaussians, and the amounts of desorbed water corresponding to each Gaussian were determined by the area under the peaks. This deconvolution of the distribution function allows quantitative characterization of the strength of interaction of water with the zeolite. Of the total of 256 water molecules desorbed, 71 of them have desorption energies of less than 45 kJ mol^{-1} (isothermal desorption when flushing with helium at 298 K). For the nonisothermal desorption, 21 water molecules desorb with an average energy of 51 kJ mol^{-1}, 111 molecules with 58 kJ mol^{-1}, 33 molecules with 68 kJ mol^{-1}, and 21 molecules with 80 kJ mol^{-1}. Deconvolution of the distribution function of water in NaY also yields 4 Gaussians centered at energies that are similar to the NaX case (see Figure 7). The less-pronounced hydrophilic properties of the NaY zeolite are clearly indicated by the fact that about 50% of adsorbed water desorbs isothermally at 298 K and that the relative amount of water that corresponds to the peak centered at 51 kJ mol^{-1} is significantly higher than in NaX. It is also characteristic that the amounts of desorbed water that correspond to the higher-energy peaks are much smaller for NaY as compared to those of NaX. Without any further information, the latter peaks are assigned to adsorbed water molecules interacting with the sodium cations, and the much smaller number of water molecules with desorption energies in this range in NaY is indicative of the smaller number of sodium cations in this zeolite.

The detailed information about the adsorption behavior of water in the NaX zeolite, obtained with adsorption isotherm and TPD techniques, that documents the existence of several different structures of adsorption complexes of water was used as starting point for the DRIFT and neutron diffraction experiments.

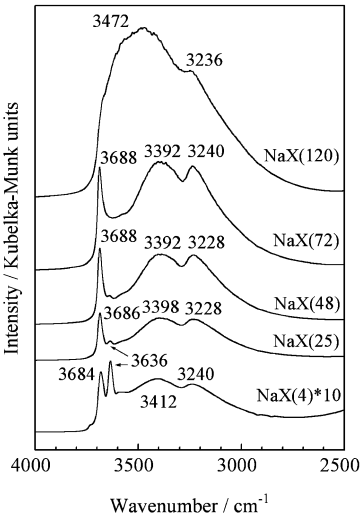

Figure 8. DRIFT spectra of adsorbed water on NaX in the OH stretching region.

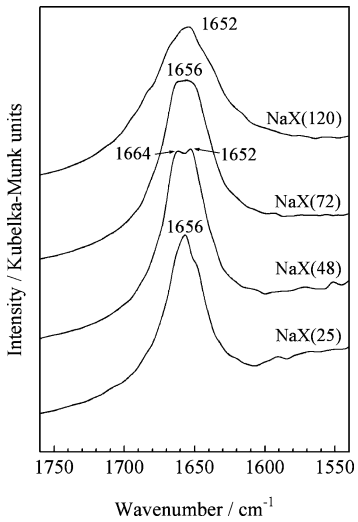

Figure 9. DRIFT spectra of adsorbed water on NaX in the HOH bending region.

DRIFT Spectroscopy. Figures 8 and 9 show the DRIFT spectra of the water-loaded NaX samples in the OH stretching and bending regions, respectively. Four major effects occur in the DRIFT spectra of water adsorbed in NaX when the loading decreases:

(a) At a loading of 120 water molecules per unit cell (NaX-(120)), two broad associate bands at 3472 and 3236 cm^{-1} are observed. The intensity of the higher-frequency band is significantly greater than that of the lower-frequency band.

(b) At a loading of 72 water molecules per unit cell (NaX-(72)), an additional sharp band appears at about 3688 cm^{-1}. There are still two broad associate bands, whereby the maximum of the higher-frequency band is downshifted to 3392 cm^{-1}. The intensity of the higher-frequency band has decreased significantly but still remains higher than the intensity of the lower-frequency band at about 3240 cm^{-1}.

(c) Upon further decrease of the water loading to 48 and 25 molecules per unit cell (NaX(48) and NaX(25), respectively), the total intensity of the DRIFT spectrum in the OH stretching

region decreases almost proportionally to the water loading. The intensity ratio of the two broad associate bands remains unchanged, while another additional sharp band appears at 3636 cm^{-1}. In the case of only 4 water molecules per unit cell, this additional sharp band is especially well noticeable.

(d) For all the above-mentioned loadings, a broad band at about 1656 cm^{-1} that exhibits some structure is observed in the HOH bending region. The half-width at half-maximum of this band increases almost linearly with the water loading.

For the interpretation of the DRIFT spectra, we chose to start with the lowest loading because the spectra at low loadings are simpler, and hence, easier to interpret due to the presence of a small number of species of adsorbed water molecules.

At a loading of 25 molecules per unit cell (NaX(25)), we observe two sharp bands (3686 and 3636 cm^{-1}) as well as two broad associate bands at 3398 and 3228 cm^{-1}. The two sharp bands could arise from the symmetric/antisymmetric combination of the relatively unperturbed OH oscillators of the same water molecule or they could also be due to OH oscillators of different water molecules located at two distinctly different positions in the cages. In the latter case, one OH bond of the water molecule would interact with framework oxygen, while the other OH bond would point into the cage. The possibility of the symmetric/antisymmetric combination can be excluded for two reasons: First, the separation between these two sharp bands (50 cm^{-1}) is too small compared with the separation between symmetric and antisymmetric stretchings in gaseous water (100 cm^{-1}). Second, if water molecules with both OH bonds unperturbed were present, we should observe an HOH bending vibration at about 1600 cm^{-1}, which is not the case in our spectra. By excluding the possibility of symmetric/antisymmetric combinations, it remains that the two sharp bands must originate from different water molecules for which one OH bond is hydrogen bonded while the other OH bond points into the cage and is almost unperturbed by hydrogen bonding. Because we observe two sharp bands, two distinct positions must exist in the cages where water molecules are located. These could be either different crystallographic positions (for example, cages of different types) or positions whose immediate environments are different because of the distribution of Na^+ ions. We recall here that migration of Na^+ ions is significantly enhanced when water is adsorbed in the zeolite.[21,22,23] Quantum mechanical computations, however, show that the free OH bond of water molecules that only donates a hydrogen bond vibrates at a higher frequency than the free OH bond of a molecule that is both hydrogen bond donor and acceptor.[54] These results offer an opportunity for assigning the two sharp bands if the two above-mentioned species of water molecules are present in the system. At an even smaller loading of 4 molecules per unit cell, the intensities of the two sharp bands are almost equal[37] (see Figure 8).

In addition to the two sharp bands, the DRIFT spectra also show two broad associate bands, even at the smallest loadings studied. The high-frequency associate band (3398 cm^{-1}) often exhibits an internal structure. The position and intensity of the high-frequency band depend on the water loading. In contrast to this behavior, the position of the low-frequency associate band is almost unchanged at 3240 cm^{-1}. At first look, one could assign the two sharp and the two associate bands to water molecules in the two distinct positions mentioned above, i.e., the sharp band at 3686 cm^{-1} and the high-frequency associate band arise from water molecules at one of the positions, and the other sharp band at 3636 cm^{-1} and the lower-frequency associate band arise from molecules at the other position. This assignment is, however, not supported by the experimental observations. When the water loading changes from 48 to 72 molecules per unit cell, the intensities of the sharp band at 3686 cm^{-1} and the two associate bands increase significantly, while the intensity of the other sharp band at 3636 cm^{-1} decreases. This implies that the high-frequency sharp band and the two associate bands are due to water molecules in identical positions, whereas the low-frequency sharp band arises from another species of adsorbed water. One possible explanation that takes into account the experimental behavior of the positions and intensities of the associate bands starts with the assumption that the associate band at 3398 cm^{-1} arises from water molecules that are hydrogen bonded. The two distinct positions of water molecules (see discussion of the two sharp bands above) could, however, only lead to a slight structuring of a broad associate band and, therefore, cannot explain the existence of the low-frequency associate band at 3240 cm^{-1}. The origin of the associate band at 3240 cm^{-1} could be explained by invoking the existence of Fermi resonance between the downshifted OH stretchings and the overtone of the HOH bending of the water molecule. Because the Fermi resonance "pushes" the bands further apart and increases the intensity of the normally weak overtone, the associate band at 3240 cm^{-1} could be the downshifted overtone of the HOH bending ($2\delta(H_2O)$; $1656 \times 2 = 3312$ cm^{-1}). The unchanged position of the low-frequency associate band is then a consequence of the fact that only those stretchings of hydrogen-bonded OH groups that lie close to the bending overtone (3312 cm^{-1}) will participate in the Fermi resonance. The higher the frequency of an OH stretching, the less its contribution to Fermi resonance with the bending overtone. We notice here, though, that the vibrations involved in the Fermi resonance (OH stretching and HOH bending overtone) change their nature and assume to some degree both stretching and bending character.[55,56]

As another possibility for explaining the existence of the two associate bands even at the lowest loadings, we consider the arguments presented by Walrafen for the interpretation of the Raman spectrum of liquid water. On the basis of the existence of exact isosbestic points in the Raman spectra, Walrafen advocated for many years the two-state model for liquid water, which assumes that OH oscillators with intact and broken hydrogen bonds coexist in water in dynamical equilibrium with each other.[57,58,59] In the original treatment of Walrafen, broken hydrogen bonds represent, in fact, severely bent or stretched O−H···O configurations whose interaction energies are below a certain threshold. The physical basis for such an interpretation is that the energy required to break the hydrogen bond is only about 20 kJ mol^{-1}, and even at room temperature, there is enough thermal energy to cause very significant fluctuations of the hydrogen bond network in water. Application of these ideas in the case of water adsorbed in zeolites implies that water−water and water−framework oxygen hydrogen bonds would be partially broken and partially intact at any moment in time. Therefore, the two associate bands could be thought of as originating from broken and intact hydrogen bonds of adsorbed water molecules whereby the low-frequency associate band corresponds to intact hydrogen bonds and the high-frequency associate band corresponds to broken hydrogen bonds. Broken hydrogen bonds considered here would not give rise to sharp bands because, although the hydrogen bond is no more intact, the corresponding OH group still interacts weakly, and hence, its stretching is perturbed with the framework oxygen atoms. Sharp bands observed at relatively low water loadings

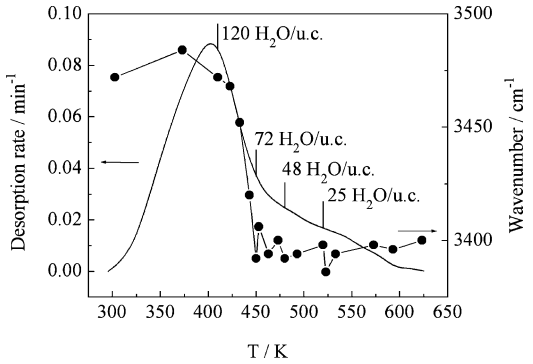

Figure 10. Relationship between the position of the high-frequency associate OH stretching band in dependence on the temperature and the course of water desorption on NaX.

are caused, as shown earlier, by almost unperturbed OH bonds of water molecules that point into the zeolite cages.

With increasing water loading to 48 and 72 molecules per unit cell, the relative intensity of the low-frequency sharp band decreases even further. There are, however, no changes of positions and the relative intensities of the high-frequency sharp band and the two associate bands. The total intensity of the OH stretching band complex, of course, increases because of the higher water content.

The presence of only one sharp band of significant intensity suggests that there is only one species of free OH oscillators, whereas the similarity of associate band positions indicates almost no change in the average hydrogen bond strength. These two facts lead us to believe that the topology of water−Na^+ complexes is similar for the three loadings of 25, 48, and 72 water molecules per unit cell, the only difference is in the size of the complexes.

Further increase of the water loading to 120 molecules per unit cell (NaX(120)) leads to drastic changes of the spectrum in the OH stretching region and to significant broadening of the HOH bending band. Many different arrangements of water molecules are now possible, and thus, the associate band at 3472 cm^{-1} and the HOH bending at 1652 cm^{-1} are significantly broadened. The upshift of the associate band from 3392 cm^{-1} at a loading of 72 molecules per unit cell to 3472 cm^{-1} at 120 molecules per unit cell indicates decrease of the average strength of hydrogen bonds. On the basis of this analysis, we conclude that, when the loading changes from 72 to 120 molecules per unit cell, some kind of "phase transition" occurs in a small temperature interval for the water inside the cages of NaX, as illustrated by the sudden change of the position of the associate band at 3500−3400 cm^{-1} (see Figure 10).

Neutron Powder Diffraction. For quantitative information concerning the refinement results, see Tables 2−5 as well as Supporting Information. Selected bond lengths and angles for the framework and the extraframework cations are listed in Table 2, whereas occupancies of the water and extraframework cation sites for NaX(0), NaX(25), NaX(48), and NaX(72) are summarized in Table 3. Selected distances between Na^+ ions and O_w of the refined structures are shown in Table 4 (distances between 2.15 and 3.7 Å were considered). Table 5 shows selected bond lengths and angles of hydrogen bonds (H bonds with distances $D-O_{acc} = 1.40-2.65$ Å, angles $O_w-D-O_{acc} > 130°$, and distances $O_w-O_{acc} = 2.30-3.35$ Å were considered).

The extraframework sodium cations were refined on five positions, the conventional SI, SI′, SII, and SIII positions as well as a SJ position, which is located in the 12-ring window between two supercages. The latter position is also described in a previous single-crystal X-ray structure determination of completely hydrated NaX zeolite.[40] All these positions are nearly similar in the refined structures and are therefore named identical.

NaX(25). In the sample NaX(25), four nonequivalent positions of water molecules were located. Three of these positions are situated in the supercages (a, b, and II*), and one is situated in the sodalite cages (II′) (see Figures 11 and 12).

The position D_2O(a) is located close to the 12-ring mean plane, which implies that around 60% of the located D_2O

TABLE 2: Selected Bond Lengths [Å] and Angles [deg] for the Framework and Extraframework Cations in the Refined Samples (T1 is the Site Assigned to Si, T2 the Site Mostly Occupied by Al)

	NaX(0)		NaX(25)		NaX(48)		NaX(72)	
	T1 atom	T2 atom	T1 atom	T2 atom	T1 atom	T2 atom	T1 atom	T2 atom
T−O1	1.635(9)	1.677(11)	1.609(8)	1.712(8)	1.627(7)	1.667(7)	1.573(8)	1.753(9)
T−O2	1.603(9)	1.734(10)	1.597(7)	1.740(8)	1.762(7)	1.607(7)	1.778(8)	1.595(9)
T−O3	1.714(9)	1.654(10)	1.730(7)	1.602(7)	1.527(6)	1.803(7)	1.568(8)	1.780(9)
T−O4	1.601(9)	1.704(10)	1.656(7)	1.699(7)	1.591(6)	1.778(7)	1.630(8)	1.682(9)
av T−O	**1.64(4)**	**1.69(4)**	**1.65(3)**	**1.69(3)**	**1.63(3)**	**1.71(3)**	**1.64(3)**	**1.70(4)**
Si−O1−Al/Si	137.2(5)		138.3(4)		137.0(4)		138.8(5)	
Si−O2−Al/Si	145.4(4)		145.3(4)		142.4(4)		142.4(4)	
Si−O3−Al/Si	142.0(5)		142.3(4)		142.0(4)		138.9(4)	
Si−O4−Al/Si	147.5(5)		145.9(4)		144.2(3)		143.4(4)	
av Si−O−Al/Si	**143.0(19)**		**141.9(16)**		**141.4(15)**		**140.9(17)**	
O1−T−O2	111.4(5)	115.5(5)	113.5(4)	112.7(4)	108.1(4)	118.2(4)	108.3(4)	115.0(5)
O1−T−O3	106.8(5)	111.9(5)	107.0(4)	113.7(4)	115.2(4)	106.3(4)	113.2(5)	103.9(5)
O1−T−O4	109.6(5)	110.5(5)	108.0(4)	110.1(4)	106.1(4)	112.7(4)	110.2(5)	109.0(5)
O2−T−O3	105.9(5)	105.8(5)	108.4(4)	107.0(4)	108.1(3)	106.4(4)	104.8(4)	110.0(5)
O2−T−O4	111.0(5)	103.9(5)	107.8(4)	101.4(4)	101.7(3)	105.5(4)	102.4(4)	107.1(5)
O3−T−O4	112.0(5)	108.7(5)	112.2(4)	111.2(4)	116.5(4)	107.2(3)	116.9(5)	112.0(5)
av O−T−O	**109.5(25)**	**109.4(25)**	**109.5(24)**	**109.4(24)**	**109.3(22)**	**109.4(23)**	**109.3(27)**	**109,5(30)**
Na(SI)−O3	2.761(5)		2.778(4)		2.789(3)		2.718(5)	
Na(SI′)−O3	2.265(6)		2.280(6)		2.295(6)		2.304(7)	
Na(SI′)−O2	2.937(6)		2.964(6)		2.976(6)		3.020(7)	
Na(SII)−O2	2.369(6)		2.366(6)		2.335(6)		2.329(7)	
Na(SII)−O4	2.923(8)		2.877(6)		2.884(6)		2.914(7)	
Na(SIII)−O4	2.609(22)		2.748(18)		2.43(4)		2.45(5)	
Na(SJ)−O1	1.88(7)		2.77(3), 2.908(23)		2.63(3), 3.04(3)		2.773(21), 3.137(21)	
Na(SJ)−O4	2.56(10)		1.98(3)		1.95(3)		2.168(19)	

TABLE 3: Site Occupancies of Extraframework Cation Sites and Water Sites for the Refined Samples in Molecules Per Unit Cell

	NaX(0)	NaX(25)	NaX(48)	NaX(72)
Na^+(SI)	1.1(3)	0.9(2)	3.6(3)	1.3(3)
Na^+(SI′)	31.3(4)	26.3(4)	26.4(4)	25.9(5)
Na^+(SII)	32 (fixed)	30.2(4)	30.0(4)	32 (fixed)
Na^+(SIII)	10.7(5)	7.6(4)	4.1(4)	3.7(5)
Na^+(SJ)	7.8(7)	22.0(6)	16.9(9)	30.4(9)
total Na^+	**83(2)**	**87(2)**	**81(2)**	**93(2)**
D_2O(a)		10.94(19)		
D_2O(b)		5.09(19)		
D_2O(c)			20.26(19)	
D_2O(d)			4.32(19)	
D_2O(e)			6.14(19)	
D_2O(f)			7.20(19)	
D_2O(g)				20.5(3)
D_2O(h)				12.1(3)
D_2O(i)				10.27(19)
D_2O(k)				9.1(3)
D_2O(II*)		0.58(10)	2.21(10)	5.47(10)
D_2O(II′)		1.63(10)	2.68(10)	8.16(10)
total D_2O	**0**	**18.2(6)**	**42.8(10)**	**65.6(13)**

TABLE 4: Selected Distances [Å] between Na^+ Ions and O_w Atoms

			NaX(25)			
		O (a)	O (b)	O (II*)		O (II′)
Na(SJ)						
Na(SIII)		3.11(2)				
Na(SII)				2.173(4)		3.055(4)
			NaX(48)			
	O (c)	O (d)	O (e)	O (f)	O (II*)	O (II′)
Na(SJ)		3.32(6)	3.67(4)			
Na(SIII)	3.32(3)	3.29(7)				
Na(SII)					2.64(5)	3.09(3)
			NaX(72)			
	O (g)	O (h)	O (i)	O (k)	O (II*)	O (II′)
Na(SJ)		3.36(3)	3.54(3)	2.76(3)		
Na(SIII)	3.24(7)					
Na(SII)		3.36(2)			2.23(2)	3.069(11)

TABLE 5: Selected Parameters of Possible Hydrogen Bonds

D atom	O_{acc}	distance D−O_{acc} [Å]	distance O_w−D [Å][a]	angle O_w−D−O_{acc} [deg]	distance O_w−O_{acc} [Å]
			NaX(25)		
D2(a)	O(a)	2.05(4)	0.96(3)	133(3)	2.79(3)
D2(a)	O4	2.28(3)	0.96(3)	151.3(25)	3.155(22)
D2(b)	O1	1.72(6)	0.96(6)	137(7)	2.62(4)
			NaX(48)		
D1(c)	O(c)	1.825(23)	0.96(2)	154.6(19)	2.724(17)
D2(c)	O1	1.773(19)	0.96(2)	147.8(18)	2.637(16)
D2(d)	O4	1.47(9)	0.96(8)	144(7)	2.32(5)
D2(e)	O1	1.95(5)	0.96(5)	161(5)	2.87(3)
D2(f)	O1	2.61(5)	0.96(5)	132.8(5)	3.34(3)
			NaX(72)		
D1(g)	O(g)	1.798(24)	0.962(23)	164.1(20)	2.735(18)
D2(g)	O1	1.763(19)	0.961(19)	170.7(17)	2.716(15)
D2(h)	O4	1.72(3)	0.96(4)	174(3)	2.679(24)
D1(i)	O(h)	1.43(4)	0.96(4)	167(3)	2.37(3)
D1(k)	O(i)	2.20(5)	0.96(4)	150(4)	3.07(4)
D1(II*)	O(h)	1.67(7)	0.96(6)	138(4)	2.47(3)

[a] Soft constrained.

molecules are situated in the 12-ring windows between two supercages (10.9 molecules per unit cell). These water molecules are coordinated to the Na(SIII) sodium ions (distance Na(SIII)−O(a) = 3.11 Å), they show possible hydrogen bonds to framework oxygen O4 (distance D2(a)−O4 = 2.28 Å) and another D_2O(a) molecule (distance D1(a)−O(a) = 2.05 Å).

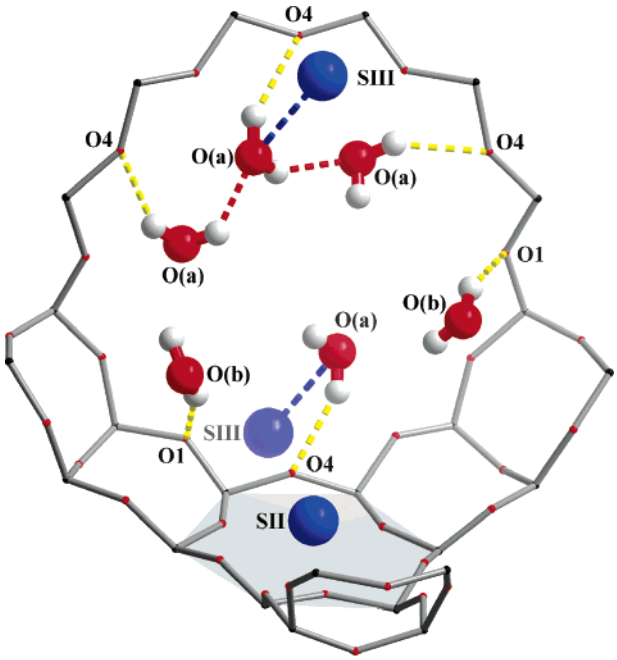

Figure 11. Location of the D_2O sites a and b in the structure NaX-(25).

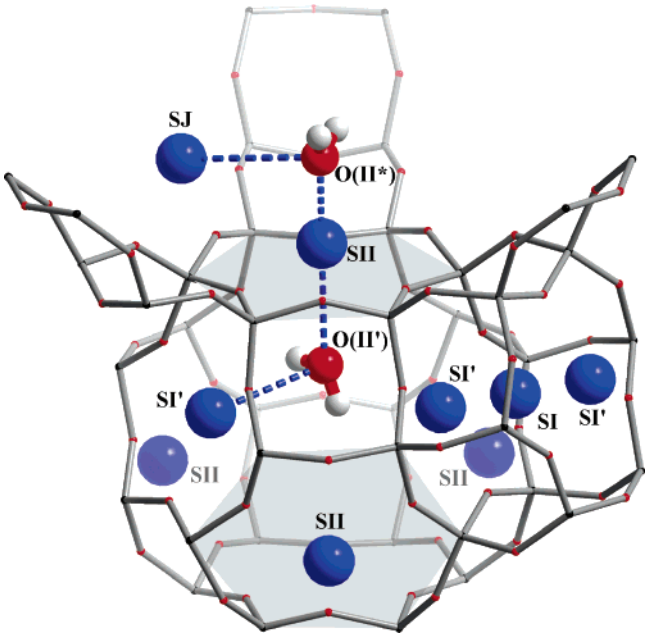

Figure 12. Location of the D_2O sites II* and II′ in the structure NaX-(25).

The water molecules D_2O(b) are apparently not coordinated to any sodium ions, but they are involved in a hydrogen bond to the framework oxygen atom O1 (distance D2(b)−O1 = 1.72 Å). The other hydrogen atom D1(b), which is arranged toward the 12-ring window, remains definitely free of hydrogen bonds. Because of the short distance of 1.18 Å between Na(SIII) and O(b), it seems to be impossible that D_2O(b) and Na(SIII) are occupied simultaneously.

The third refined position for water in the supercage D_2O-(II*) is occupied by 0.6 water molecules per unit cell. The D_2O molecules on this position are coordinated to the SII cations (distance Na(SII)−O(II*) = 2.17 Å) and seem not to be involved

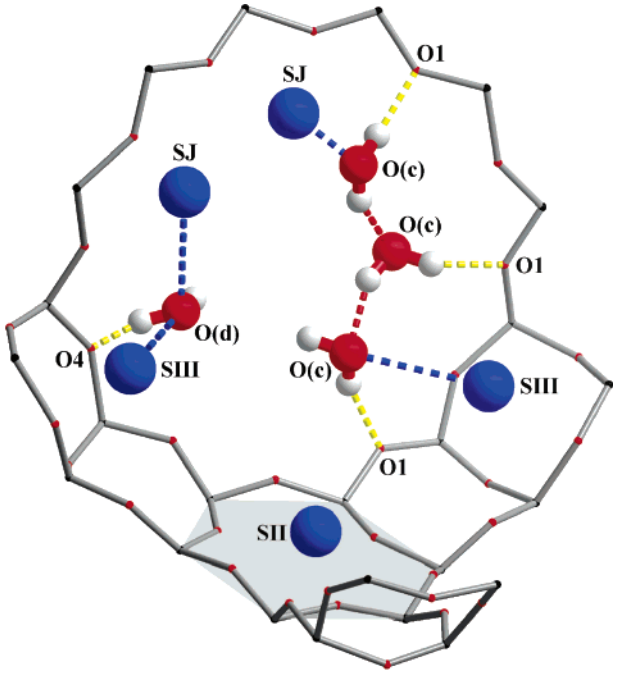

Figure 13. Location of the D_2O sites c and d in the structure NaX-(48).

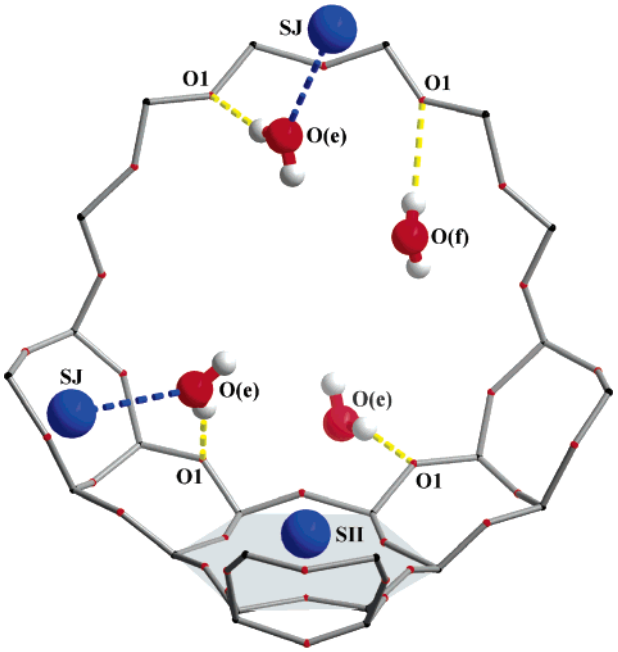

Figure 14. Location of the D_2O sites e and f in the structure NaX-(48).

in any hydrogen bonds. These molecules are disordered about the 3-fold axes.

In all samples, we found also some water molecules D_2O-(II′) in the sodalite cages (NaX(25): 1.6 molecules per unit cell) that show weak interaction with the SII cations (NaX(25): distance Na(SII)−O(II′) = 3.06 Å) and no hydrogen bonding. These D_2O molecules are also disordered about the 3-fold axes.

NaX(48). In the sample NaX(48), six D_2O positions were refined (see Figures 13 and 14). The positions D_2O(c), D_2O(d), and D_2O(f) are located close to the 12-ring mean plane (20.3, 4.3, and 7.2 molecules per unit cell, respectively). Counted together, water molecules in these three positions represent about 74% of the total number of localized D_2O molecules. The position D_2O(c) is almost similar to the position D_2O(a) in NaX-(25). Both of the water molecules in the 12 rings display possible hydrogen bonds to framework oxygen atoms O1 or O4, respectively. D_2O(c) displays a further possible hydrogen bond to another D_2O(c) molecule. On the D_2O(d) positions, one hydrogen atom D1(d) definitely remains free of any hydrogen bonding. D_2O(d) are coordinated to Na(SJ) (distances O(d)−Na(SJ) = 3.32 Å). D_2O(c) and D_2O(d) may also be coordinated to Na(SIII) (distances O(c)−Na(SIII) = 3.32 Å, O(d)−Na(SII) = 3.29 Å). One of the hydrogen atom D1(f) of water molecules on the D_2O(f) positions definitely remains free of any hydrogen bonding. The other hydrogen atom D2(f) shows a bifurcated hydrogen bond to framework oxygen atoms O1 and O4 (see Figure 14). D_2O(f) seems not to be coordinated to any sodium ions.

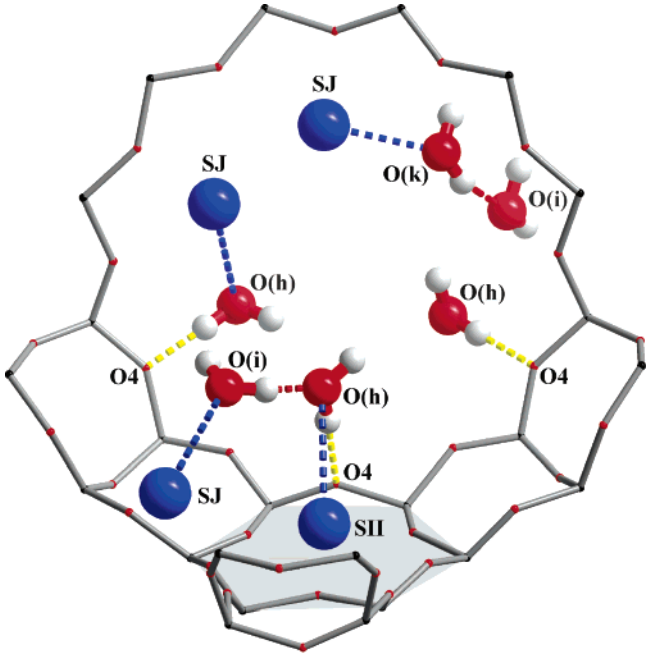

Figure 15. Location of the D_2O sites h, i, and k in the structure NaX-(72).

The D_2O molecules on the D_2O(e) positions are located in the inner supercage near Na(SIII), showing a possible hydrogen bond to framework oxygen O1. The other hydrogen atom D1-(e) remains free of hydrogen bonds. The molecules on D_2O(e) positions are coordinated to Na(SJ) (distances O(e)−Na(SJ) = 3.67 Å).

The fifth refined position for water in the supercage D_2O-(II*) is occupied by 2.2 water molecules per unit cell and is essentially similar to the D_2O(II*) position in NaX(25). Also, the D_2O(II′) position (2.7 molecules per unit cell) in the sodalite cages appears similar to its homonymous position in NaX(25).

NaX(72). Six D_2O positions were refined in the NaX(72) sample (see Figures 15 and 16). The water molecules on D_2O-(g) positions, which have the highest occupancy factor (20.5 molecules per unit cell), are located in the 12-ring windows similar to positions D_2O(c) in NaX(48) and D_2O(a) in NaX-(25), respectively. The water molecules on this position can interact with a sodium ion on SIII position (distance Na(SIII)−O(g) = 3.24 Å). In the case of D_2O (g) positions, one of the D atoms points toward the O1 framework oxygen and forms a hydrogen bond with it, whereas the other D atom remains localized in the 12-ring plane. The consequence of such a coordination is that, when several neighboring position in the 12-ring are occupied, hydrogen bonds between D_2O molecules are formed in addition to hydrogen bonds to the O1 framework

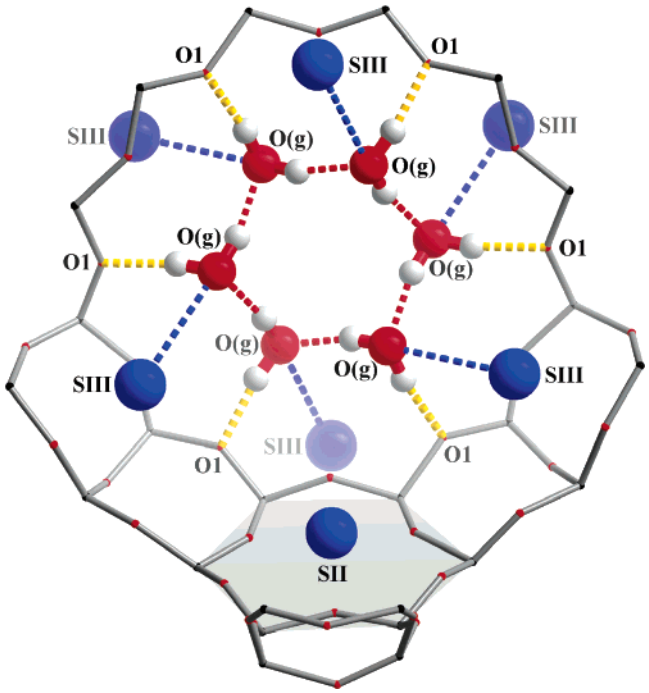

Figure 16. Location of the D_2O site g in the structure NaX(72).

oxygen. If all the positions are occupied, cyclic D_2O hexamers form in the 12-rings. This structural motif that occurs in ice, Ih, has been recently observed in water clusters trapped in liquid helium droplets and solid parahydrogen.[60,61] In the case of water adsorbed on the NaX zeolite, additional stabilization of the hexamer occurs because of the hydrogen bonding to O1 framework oxygen atoms. When the hexamer forms, the Na(SJ) position cannot be occupied anymore, but the coordination of D_2O molecules to Na(SIII) is still retained. The hexamer can also form in the case of the D_2O(c) position in NaX(48) and of D_2O(a) in NaX(25). Interestingly, these two positions along with D_2O(g) have the highest occupancies in NaX(25), NaX(48)m and NaX(72), respectively.

The D_2O(h) position is located close to the 12-ring mean plane. The D_2O(h) molecules (12.1 molecules per unit cell) are coordinated to the SJ cations (distance Na(SJ)−O(h) = 3.36 Å). In addition, they can interact with SII cations (distance Na(SII)−O(h) = 3.36 Å). The molecules on the position D_2O(h) are also involved in the hydrogen-bonding system. Possible hydrogen bonds are observed to framework oxygen atom O4.

The water molecules D_2O(i) (10.3 molecules per unit cell) are located in the inner supercages between Na(SII) and Na(SIII) and are coordinated to sodium ions on Na(SJ) position (distance Na(SJ)−O(i) = 3.54 Å). They show one possible hydrogen bond to water molecules D_2O(h). This water position was already characterized in former X-ray experiments with a sample containing 33 H_2O molecules per unit cell.[38] Because of the hydrogen atom, D2(i) is arranged toward the Na(SIII) position, and the D_2O(i) position cannot be occupied if Na(SIII) is occupied.

The water molecules D_2O(k) (9.1 molecules per unit cell) are coordinated to Na(SJ) (distance Na(SJ)−O(k) = 2.76 Å) and are located in the 12-ring windows near D_2O(g). Probably, D_2O(k) cannot be occupied if the neighboring Na(SIII) is occupied. Further geometrical considerations strongly suggests that D_2O(k) can interact through only one of its hydrogen atoms (D1(k)) with another water molecule D_2O(i). The other hydrogen atom D2(k) seems to show no interaction with other water or framework oxygen atoms. Furthermore, D_2O(k) cannot be occupied if a D_2O(g) 6-ring (see Figure 16) is realized.

The D_2O(II*) and D_2O(II′) molecules are located on similar positions, such as in the NaX(48) and NaX(25) samples, and are also disordered about the 3-fold axes. These positions are occupied by 5.5 and 8.2 water molecules per unit cell, respectively, which implies that all the sodalite cages contain one such water molecule on average. In contrast to D_2O(II*) positions in NaX(48) and NaX(25) samples, water molecules on such positions in NaX(72) show a possible hydrogen bond to D_2O(h) molecules, but not to any framework oxygen atoms.

One can imagine many different arrangements of water molecules and sodium ions in the supercages are possible. Furthermore, it is plausible that the arrangement is dependent on the arrangements in the neighboring supercages (almost all water molecules are located in the environment of the 12-ring windows). This consideration leads to multiple "super structures" that can be realized. At the moment, we cannot handle this because further work (e.g., MC calculations) is necessary to get more information.

Conclusions

From adsorption isotherm measurements of water in NaX and calculation of the total pore volume, we can conclude that water molecules, unlike for example N_2, can enter both the supercages and the sodalite cages. Energy distribution functions calculated from the adsorption isotherm show a maximum at 49 kJ mol^{-1} and have a width of about 15 kJ mol^{-1}. The energy value of the maximum is close to evaporation heat of liquid water (ΔH = 44 kJ mol^{-1} at 298 K), which implies that the adsorption isotherm mostly contains information about relatively weakly bonded water species present at relatively high loadings. Temperature-programmed desorption, on the other hand, is very well suited to studying the low loading region. Desorption energy distribution functions calculated from the desorption curve of water in NaX could be fitted with 4 Gaussians centered at 51, 58, 68, and 80 kJ mol^{-1}, with amounts under each peak of 21, 111, 33, and 21 water molecules, respectively. Energy distribution functions for water in NaY could also be fitted with 4 Gaussians at similar positions, but in this case, more water molecules correspond to the low-energy peaks and less to the high-energy Gaussian compared with NaX. In simple language, this result shows that NaX is more hydrophilic than NaY, which in addition to the larger number of cations in NaX compared with NaY, could also be caused by different, energetically more favorable structures of adsorption complexes of water in NaX.

DRIFT spectra obtained in situ during the course of nonisothermal desorption of water in NaX change dramatically with decreasing water loading. We observed two broad associate bands at 3472 and 3236 cm^{-1} for a loading of 120 H_2O molecules per unit cell. The high-frequency feature downshifts to 3392 cm^{-1} when the water amount decreases to 72 molecules. This sudden shift occurs in a narrow temperature interval and could signify some kind of "phase transition" for the water inside the zeolite cavities. While the positions of the two associate bands remain unchanged from 72 water molecules downward, a sharp feature at 3688 cm^{-1} is observed at this loading, which is accompanied by a similar sharp band at 3636 cm^{-1} for water amounts of 48 and 25 molecules per unit cell. For all the above-mentioned loadings, there is an H−O−H bending at about 1656 cm^{-1}, which ensures that the observed sharp features are not due to bridging OH groups of some kind, but rather due to OH bonds of water molecules that are not engaged in hydrogen bonding. The two sharp features observed at low loadings should

be due to water molecules in slightly different environments for which one OH bond is hydrogen bonded while the other OH bond points into the cage and is almost unperturbed by hydrogen bonding. To explain the origin of the two associate bands present at every water loading, we considered the possibility of Fermi resonance between the overtone of the H−O−H bending and the downshifted OH stretchings of the water molecules as well as the existence of intact and partially broken hydrogen bonds, which would give rise to associate bands at different frequencies.

Neutron diffraction studies carried out for four different loadings of water in NaX reveal several possible arrangements of water molecules with respect to the zeolite framework and Na^+ cations. For the smallest loading of 25 water molecules per unit cell, the majority of D_2O molecules are located in D_2O-(a) and D_2O(b) positions of which a D_2O(a) molecule has two hydrogen bonds to O4 framework oxygen and another D_2O(a) molecule, respectively, whereas a D_2O(b) molecule has a hydrogen bond to O1 framework oxygen and a free OD bond that does not participate in hydrogen bonding. For the other two loadings of 48 and 72 water molecules per unit cell, it is characteristic that two positions, D_2O(c) and D_2O(g), respectively, which are similar to D_2O(a), have the highest occupancies. If all the adjacent positions of these kinds are occupied, cyclic water hexamers will form, which are further stabilized by hydrogen bonding to framework oxygen. Several other positions have been refined for the samples with 48 and 72 water molecules per unit cell. The positions D_2O(d) and D_2O(f) in the sample with 48 water molecules per unit cell are located in the 12-rings and have both one OD bond engaged in hydrogen bonding and one other free OD bond, whereas molecules in D_2O(e) positions are coordinated to sodium cations in SIII positions and also have one free and one hydrogen-bonded OD bond. In the case of the NaX sample loaded with 72 water molecules per unit cell, the positions D_2O(h), D_2O(i), and D_2O-(k) are located in the 12-rings and have two, one, and one hydrogen-bonded OD bonds, respectively. In addition to the above-mentioned positions, there are two other locations of D_2O molecules, D_2O(II*), and D_2O(II′) located in the supercages and in the sodalite cages, respectively, are found in all samples. These latter positions, however, have low occupancies, no hydrogen bonds, and they are disordered about the 3-fold axes.

The presence of water molecules with hydrogen-bonded and free OD bonds is in good agreement with the DRIFT spectra, which show broad associate bands due to hydrogen-bonded water molecules and two sharp bands due to OD bonds free of hydrogen bonding. An attempted assignment of the two sharp bands would be as follows. Water molecules in (a), (c), or (g) positions donate one hydrogen bond to an O1 or O4 framework oxygen atom. If, however, a molecule in such a position would also donate a second hydrogen bond to a neighboring molecule in a similar position, the last water molecule would have a free OH bond and be both a donor and acceptor of hydrogen bonds. On the basis of the results of quantum mechanical computations, the first species (only donor) will give rise to a higher-frequency OH stretch than the donor−acceptor species. With increasing water loading and formation of cyclic hexamers, the number of free OH groups on donor−acceptor water molecules will steadily decrease until it becomes zero. This prediction is in qualitative agreement with the experimental observed decrease of the intensity of the low-frequency OH stretch with increasing water loading.

Quantitative comparison of the results is unfortunately not possible for several reasons. First, we cannot quantify the number of water molecules with free OH bonds in the DRIFT spectra because we do not know the relative absorption coefficients for the hydrogen-bonded and non-hydrogen-bonded OH oscillators. The situation is complicated even more by the fact that the hydrogen-bonded molecules are not one single species and effects such as Fermi resonance or partially broken hydrogen bonds might affect the intensity. Another issue is the very different temperatures in which DRIFT and neutron diffraction studies were carried out. In the case of the DRIFT studies, the high temperatures (473 K and above) required to partially desorb water will cause significant occupation of higher-energy states with partially broken hydrogen bonds, whereas in the neutron diffraction measurements carried out at 5 K, water molecules will be trapped at low-energy positions.

Acknowledgment. We thank the Institut Max von Laue−Paul Langevin (Grenoble, France) for awarding beamtime and financial support for the neutron diffraction experiments. We also thank L. Moschkowitz (Institute of Experimental Physics I, University of Leipzig, Germany) for preparing the D_2O-loaded samples.

Supporting Information Available: Fractional coordinates, isotropic displacement factors, and occupancies for all refined samples. Rietveld plots for NaX(0), NaX(25), and NaX(48). CIF files for NaX(0), NaX(25), NaX(48), and NaX(72). Whole powder pattern for NaX(120). This material is available free of charge via the Internet at http://pubs.acs.org.

References and Notes

(1) Breck, D. W. *Zeolite Molecular Sieves, Structure, Chemistry, and Use*; John Wiley & Son: New York, 1974.
(2) *Introduction to Zeolite Science and Practice*; van Bekkum, H., Flanigen, E. M., Jacobs, P. A., Jansen, J. C., Eds.; *Stud. Surf. Sci. Catal.*; Elsevier: Amsterdam, 2001; Vol. 137.
(3) Barrer, R. M. *Zeolites and Clay Minerals as Sorbents and Molecular Sieves*; Academic Press: London, 1978.
(4) Venuto, P. B. *Stud. Surf. Sci. Catal.* **1997**, *105*, 811−852.
(5) Weitkamp, J. *Solid State Ionics* **2000**, *131*, 175−188.
(6) Bertsch, L.; Habgood, H. W. *J. Phys. Chem.* **1963**, *67*, 1621−1628.
(7) Angell, C. L.; Schaffer, P. C. *J. Phys. Chem.* **1965**, *69*, 3463−3470.
(8) Vucelic, V.; Vucelic, D.; Karaulic, D.; Susic, M. *Thermochim. Acta* **1973**, *7*, 77−85.
(9) Dzhigit, O. M.; Kiselev, A. V.; Mikos, K. N.; Muttik, G. G.; Rahmanova, T. A. *Trans. Faraday Soc.* **1971**, *67*, 458−467.
(10) Drebushchak, V. A. *J. Therm. Anal. Calorim.* **1999**, *58*, 653−662.
(11) Yang, S.; Navrotsky, A. *Microporous Mesoporous Mater.* **2000**, *37*, 175−186.
(12) Olson, D. H.; Haag, W. O.; Borghard, W. S. *Microporous Mesoporous Mater.* **2000**, *35*−*36*, 435−446.
(13) Rozwadowski, M.; Wloch, J.; Erdmann, K.; Kornatowski, J. *Langmuir* **1993**, *9*, 2661−2664.
(14) Halasz, I.; Kim, S.; Marcus, B. *Mol. Phys.* **2002**, *100*, 3123−3132.
(15) Pichon, C.; Methivier, A.; Simonot-Grange, M.; Baerlocher, C. *J. Phys. Chem. B* **1999**, *103*, 10197−10203.
(16) Hunger, B.; Heuchel, M.; Matysik, S.; Beck, K.; Einicke, W.-D. *Thermochim. Acta* **1995**, *269/270*, 599−611.
(17) Hunger, B.; Matysik, S.; Heuchel, M.; Geidel, E.; Toufar, H. *J. Therm. Anal.* **1997**, *49*, 553−565.
(18) Hunger, B.; Klepel, O.; Kirschhock, C.; Heuchel, M.; Toufar, H.; Fuess, H. *Langmuir* **1999**, *15*, 5937−5941.
(19) Kirmse, A.; Kärger, J.; Stallmach, F.; Hunger, B. *Appl. Catal., A* **1999**, *188*, 241−246.
(20) Mortier, W. J. *Compilation of Extraframework Sites in Zeolites*; Butterworth & Co.: London, 1982.
(21) Norby, P.; Poshni, F. I.; Gualtieri, A. F.; Hanson, J. C.; Grey, C. P. *J. Phys. Chem. B* **1998**, *102*, 839−856.
(22) Sani, A.; Cruciani, G.; Gualtieri, A. F. *Phys. Chem. Miner.* **2002**, *29*, 351−361.
(23) Doebelin, N.; Armbruster, T. *Microporous Mesoporous Mater.* **2003**, *61*, 85−103.
(24) Ellison, E. H. *J. Phys. Chem. B* **1999**, *103*, 9314−9320.

(25) Hutson, N. D.; Zaji, S. C.; Yang, R. T. *Ind. Eng. Chem. Res.* **2000**, *39*, 1775−1780.
(26) Sultana, A.; Loenders, R.; Monticelli, O.; Kirschhock, C.; Jacobs, P. A.; Martens, J. A. *Angew. Chem.* **2000**, *112*, 3062−3066.
(27) Koodanjeri, S.; Ramamurthy, V. *Tetrahedron Lett.* **2003**, *44*, 1615−1618.
(28) Komori, Y.; Hayashi, S. *Langmuir* **2003**, *19*, 1987−1989.
(29) Komori, Y.; Hayashi, S. *Chem. Mater.* **2003**, *15*, 4598−4603.
(30) Channon, Y. M.; Catlow, C. R.; Gorman, A. M.; Jackson, R. A. *J. Phys. Chem. B* **1998**, *102*, 4045−4048.
(31) Fois, E.; Gamba, A.; Tabacchi, G.; Quartieri, S.; Vezzalini, G. *Phys. Chem. Chem. Phys.* **2001**, *3*, 4158−4163.
(32) Fois, E.; Gamba, A.; Tabacchi, G.; Quartieri, S.; Vezzalini, G. *J. Phys. Chem. B* **2001**, *105*, 3012−3016.
(33) Larin, A. V.; Trubnikov, D. N.; Vercauteren, D. P. *Int. J. Quantum Chem.* **2003**, *92*, 71−84.
(34) Demontis, P.; Stara, G.; Suffritti, G. B. *J. Phys. Chem. B* **2003**, *107*, 4426−4436.
(35) Bussai, C.; Fritzsche, S.; Haberlandt, R.; Hannongbua, S. *J. Phys. Chem. B* **2003**, *107*, 12444−12450.
(36) Beta, I. A.; Böhlig, H.; Hunger, B. *Thermochim. Acta* **2000**, *361*, 61−68.
(37) Beta, I. A.; Böhlig, H.; Hunger, B. *Phys. Chem. Chem. Phys.* **2004**, *6*, 1975−1981.
(38) Kirschhock, C. E. A.; Hunger, B.; Martens, J.; Jacobs, P. A. *J. Phys. Chem. B* **2000**, *104*, 439−448.
(39) Olson, D. H. *J. Phys. Chem.* **1970**, *74*, 2758−2764.
(40) Calestani, G.; Bacca, G.; Andreetti, G. D. *Zeolites* **1987**, *7*, 54−58.
(41) Rietveld, H. M. *J. Appl. Crystallogr.* **1969**, *2*, 65−71.
(42) Larson, A. C.; Von Dreele, R. B. *General Structure Analysis System (GSAS)*; Los Alamos National Laboratory Report LAUR 86-748, 2000.
(43) Favre-Nicolin, V.; Cerny, R. *J. Appl. Crystallogr.* **2002**, *35*, 734−743.
(44) Sing, K. S. W.; Everett, D. H.; Haul, R. A. W.; Moscou, L.; Pierotti, R. A.; Roquerol, J.; Siemieniewska, T. *Pure Appl. Chem.* **1985**, *57*, 603−619.
(45) Dubinin, M. M.; Zhukovskaya, E. G.; Murdmann, K. O. *Izv. Akad. Nauk SSR, Ser. Khim.* **1962**, 760−769.
(46) Heidler, R.; Janssens, G. O. A.; Mortier, W. J.; Schoonheydt, R. A. *J. Phys. Chem.* **1996**, *100*, 19728−19734.
(47) Jaroniec, M.; Madey, R. *Physical Adsorption on Heterogeneous Solids;* Elsevier: Amsterdam, 1988.
(48) Rudzinski, W.; Everett, D. H. *Adsorption of Gases on Heterogeneous Surfaces;* Academic Press: London, 1992.
(49) Bräuer, P. *Wiss. Zeitschrift Friedrich-Schiller-Univ. Jena, Math.-Naturwiss. Reihe.* **1976**, *25*, 813−823.
(50) Hobson, J. P. *Can. J. Physics* **1965**, *43*, 1941−1950.
(51) Szombathely, M. v.; Bräuer, P.; Jaroniec, M. *J. Comput. Chem.* **1992**, *13*, 17−32.
(52) *Handbook of Chemistry and Physics*, 75th ed.; CRC Press: Boca Raton, Ann Arbor, London, Tokyo, 1994.
(53) Koch, K.; Hunger, B.; Klepel, O.; Heuchel, M. *J. Catal.* **1997**, *172*, 187−193.
(54) Lee, H. M.; Suh, S. B.; Lee, J. Y.; Tarakeshwar, P.; Kim, K. S. *J. Chem. Phys.* **2000**, *112*, 9759−9772.
(55) Vinogradov, S. N.; Linnell, R. H. *Hydrogen Bonding;* Van Nostrand Reinhold Company: New York, 1971.
(56) Klose, M.; Naberuchin, J. I. *Wasser, Struktur und Dynamik;* Akademie-Verlag: Berlin, 1986.
(57) Walrafen, G. E. In *Water: A Comprehensive Treatise*; Franks, F., Ed.; Plenum: New York, 1972; Vol. 1, Chapter 5.
(58) Walrafen, G. E.; Hokmabadi, M. S.; Yang, W.-H. *J. Chem. Phys.* **1986**, *85*, 6964−6969, 6970−6982.
(59) Walrafen, G. E. In *Structure of Water and Aqueous Solutions*; Luck, W. A. P., Ed.; Verlag Chemie: Weinheim, 1974.
(60) Nauta, K.; Miller, R. E. *Science* **2000**, *287*, 293−295.
(61) Fajardo, M. E.; Tam, S. *J. Chem. Phys.* **2001**, *115*, 6807−6810.